THE JOURNAL OF PHYSICAL CHEMISTRY C

ACS AUTHORCHOICE

pubs.acs.org/JPCC Article

Synthesis and Shape Manipulation of Anisotropic Gold Nanoparticles by Laser Ablation in Solution

Valentina Piotto, Lucio Litti,* and Moreno Meneghetti*

Cite This: J. Phys. Chem. C 2020, 124, 4820–4826

Read Online

ACCESS | Metrics & More | Article Recommendations | Supporting Information

ABSTRACT: Anisotropic gold nanostructures are attracting attention due to the strong correlation between their shape and the localized surface plasmon resonances, which allows tuning their optical responses through morphological optimizations. Laser ablation synthesis in solution usually produces stable gold nanospheres colloids without any surfactant, which is important for their easy functionalization. Nevertheless, obtaining anisotropic nanoparticles with this technique is still a challenge, and few examples show that a postsynthesis approach is usually required. We show that a single pulse laser ablation allows the synthesis of anisotropic branched gold nanoparticles through careful control of the number of laser pulses interacting with the generated nanoparticles. It is shown that the very first pulses considerably affect the morphology of the ablated nanomaterial. Moreover, also the fluence above the ablated target is found to have an important role in the final nanoparticle morphology. The study of the interaction between the nanostructures and the laser pulses is achieved using an inflow setup. The optical extinction behavior of the produced anisotropic gold nanostructures was rationalized using boundary element method (BEM) based calculations, by considering the contributions from several morphologies, which were found to be in good agreement with experimental observations.

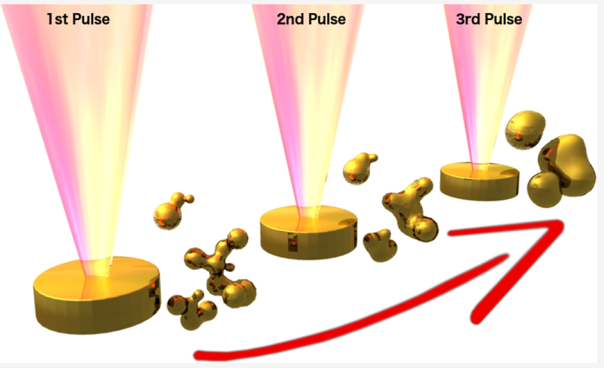

INTRODUCTION

Anisotropic gold nanostructures are attracting wide interest for their optical properties, which can span the entire visible and near-infrared (vis–NIR) spectral region. Interesting applications of these nanostructures exploit the near-field enhancement of electromagnetic fields due to localized surface plasmon excitation, like surface-enhanced Raman scattering (SERS). Nanostructure shapes can be studied for optimal excitation as in the case of sensors for nanomedicine applications[1,2] where exciting light has to be chosen in the near-infrared biological window. Anisotropic nanostructures are interesting because they show, with respect to spherical ones, several hot spots, namely, regions with high near-field electromagnetic amplifications[3] found also in nanostructures like nanoparticle aggregates,[4] bypiramids,[5] rods,[6] cubes,[7] nanostars,[3,8] and nanoworms.[9] The control and manipulation of shape and anisotropy at the nanoscale is well established using wet chemistry approaches, such as in the synthesis of nanotriangles through intermediate seeds,[10] gold nanorods synthesis mediated by CTAB[11] or also combined with Ag^+ ions,[12] or gold nanostars grown on seeds using $HAuCl_4$ and poly(vinyl pyrrolidone) (PVP).[13] All of these approaches are mostly based on the selective growth of some crystal faces, using a wide variety of capping agent or, at least, stabilizing species to stop the growth and avoiding coalescence and aggregation.

Laser ablation synthesis in solvents (LASiS) is a clean top–down approach for the production of colloids that does not need any chemicals for stabilizing the synthesized nanostructures because of their native charge. This is an advantage for many applications, particularly when the nanostructures have to be functionalized, because any exchange reaction between stabilizing molecules and those of interest is not required, or when clean surfaces are important, like for larger SERS signals.[14,15] Despite the clear advantages of this technique for the synthesis of nanoparticles, the control over their dimension and shape is poor. LASiS synthesis usually produces spherical shapes, which, as recalled above, show less interesting properties. Several studies have been presented that explore the role of solvent composition,[16,17] laser wavelength,[18] pulse duration,[19,20] repetition rate,[21] or energy fluence.[22] However, controlling the different stages of the nanoparticle synthesis, from the plasma plume formation to the collapse of the cavitation bubbles,[23] is a challenging task because different steps hardly reach thermodynamic equilibrium. Few studies report the possibility of obtaining anisotropic gold nanostruc-

Received: November 18, 2019
Revised: January 27, 2020
Published: January 30, 2020

https://dx.doi.org/10.1021/acs.jpcc.9b10793
J. Phys. Chem. C 2020, 124, 4820–4826

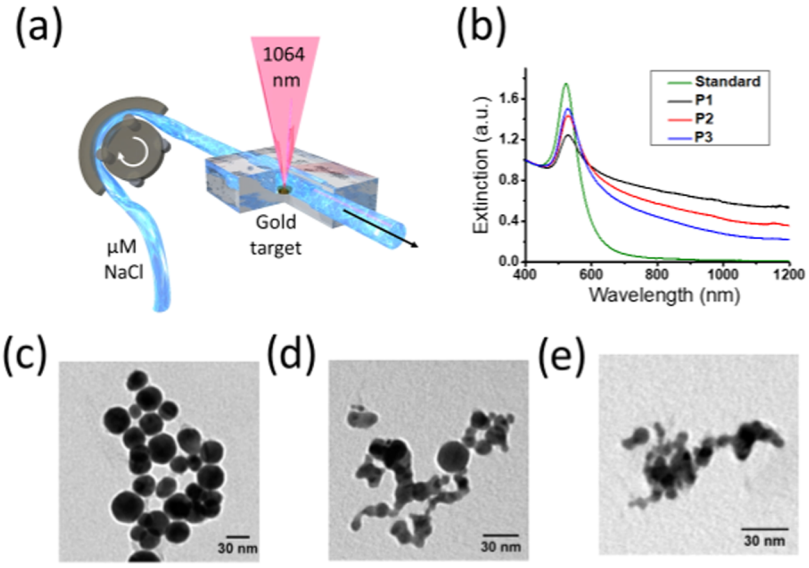

Figure 1. (a) Setup scheme representing the inflow laser ablation system. (b) Extinction spectra of samples P1, P2, and P3, normalized at 400 nm and compared to a solution of gold nanoparticles obtained in a static standard synthesis. (c–e) TEM images of respectively gold nanoparticles obtained in static standard ablation, branched nanoparticle (P1 sample), and reshaped branched nanoparticle (P3 sample).

tures due to postproduction irradiation.[24−27] Here, we present a one-step synthesis of highly anisotropic nanostructures with the laser ablation process when the synthesis is obtained by controlling the number of laser pulses, which interact with the produced nanoparticles. This was possible using an in-flow system, which allows controlling the time in which the produced nanoparticles are resident within the irradiated region. Moreover, it will be shown how the morphology of the nanoparticles is influenced by the laser fluence.

EXPERIMENTAL SECTION

Materials and Instruments. Laser ablation was carried out with a Q-Smart 450 Nd/YAG laser (6 ns, 1064 nm). A 99.999% pure gold was used for the target in the form of a disk of 5 mm diameter and 2 mm thickness. An M 045 (Techma gmp) peristaltic pump was used with 3.2 mm internal diameter Tygon tubes and operating at 0.125 mL/s. The ablation cells for the inflow system were made of Teflon, with a linear geometry and channels of 5 mm width and 5 mm (LV cell) height, as schematized in Figure 5. In the HV cell, the height was increased to 20 mm. The upper surface of the cells was covered with a micro cover glass. Dynamic light scattering (DLS) measurements were performed with a Malvern Instrument Zetasizer Nano operating with a 633 nm He−Ne laser. Transmission electron microscopy (TEM) images were collected at 100 kV with an FEI TECNAI G2 electron microscope. Optical characterization was performed with an Agilent Cary 5000 UV−vis−NIR spectrometer using quartz cuvettes. All of the chemicals were purchased from Sigma-Aldrich if not differently specified.

Laser Ablation Synthesis in "Standard Condition". Standard gold nanoparticle synthesis was carried out by focusing the laser pulses on a gold target, fixed at the bottom of a cylindrical glass cell of 2 cm diameter. A 10 μM NaCl aqueous solution was used as solvent over the target. The liquid level above the target was set to 2 cm and solvent flux or mechanical stirring was not present. The fluence was set at 2 J/cm^2 on the target with a spot diameter of Ø = 1 mm using a lens of 7.5 cm focal length, the repetition rate of 15 Hz, and the ablation proceeded for 20 min.

Laser Ablation Synthesis with the Inflow System. The P1, P2, and P3 samples were obtained with an inflow system using a peristaltic pump and setting the liquid flow at 7.5 mL per minute. A 10 μM NaCl aqueous solution was used as solvent. The laser repetition rate was changed from 5 Hz (P1 sample) to 10 Hz (P2 sample) and to 15 Hz (P3 sample). Given the liquid flow and the different pulse frequencies, the liquid volume flowing above the target received one, two, or three pulses before being completely flowed forward. The fluence was set at 2 J/cm^2 on the target, which is not moved, as in most usual ablation setup, with respect to the laser beam.

Looped Laser Ablation Synthesis. To reproduce, with the inflow system, the standard synthesis in which the nanoparticles receive multiple laser pulses, a closed-circuit was used. The Tygon tubes were closed in a loop so that the peristaltic pump fluxed the same colloidal solution multiple times inside the ablation cell above the target. At each loop, the solution enriched in particles and, at the same time, the previously synthesized particles were irradiated again. In the so-called "low volume cell" (LV), the ablation chamber was 0.5 cm high, while in the "high volume cell" (HV), it was increased to 2 cm. The fluence was set at 2 J/cm^2 on the target and the repetition rate at 15 Hz.

Standard Irradiation of LV and HV Samples. LV and HV samples, obtained through looped laser ablation, were then irradiated in static condition. In this case, the same cell of the static standard ablation was used and the laser beam was focused near the bottom of the cell, where the target is usually placed. For reproducing standard ablation conditions, the frequency of the laser and the fluence were set at 15 Hz and 2 J/cm^2, and the solution flux was not present. The irradiation was stopped after 180 min and UV−vis spectra of the solution were collected at time 0, 15, 30, 120, and 180 min to show the evolution of each sample.

Boundary Element Method (BEM) Simulation. Boundary element method (BEM) simulation was carried out using the libraries from Hohenester et al.,[28,29] implemented in

https://dx.doi.org/10.1021/acs.jpcc.9b10793
J. Phys. Chem. C 2020, 124, 4820−4826

Matlab R2017b to arrange the complex structures created with Blender 2.8. Extinction, scattering, and absorption cross sections as well as the least-squares linear regression of the experimental data with the simulated data set, were calculated following the same approach reported in a previous study.[4]

RESULTS AND DISCUSSION

Laser ablation of a target under solvents usually produces nanospheres because uncontrolled fusion and further ablation of the particles take place after the nanomaterials are first ablated from the target. The control of the interaction between laser pulses and the ablated particles is an important step in the synthesis and allows controlling fusion and further ablation processes. An inflow system, sketched in Figure 1a, was implemented within the laser ablation setup to control the number of laser pulses that interact with the solution volume flowing above the target. The inflow system consists of a low volume cell (LV cell, 5 mm height over the irradiated area) in which the μ-molar NaCl solution was flowed by a peristaltic pump. By setting the solution flow rate at 7.5 mL per minute and increasing the laser repetition frequency, it is possible to control the number of pulses hitting the solution over the gold target before it flows away. Repetition rates of 5, 10, and 15 Hz were used for hitting the volume over the target with 1, 2, and 3 pulses (samples P1, P2, and P3), respectively.

P1, P2, and P3 samples were characterized by TEM, DLS, and vis−NIR spectra and compared with gold nanoparticles obtained in static standard conditions, in which the target, and the solution over it, receives thousands of pulses in 20 min. The nanoparticles obtained in a standard experiment are spherical (see Figure 1c), with a diameter distribution (by TEM) centered at 25 nm (Figure 2a) and a narrow plasmon

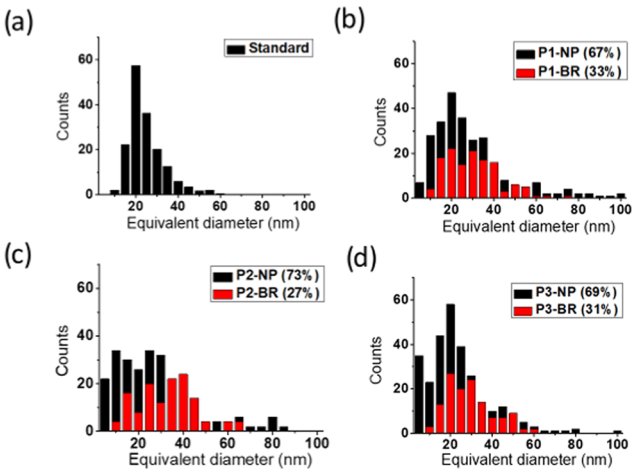

Figure 2. TEM dimensional distribution of spherical nanoparticles (NP) and branched nanostructures (BR) for static standard ablated gold nanoparticles samples (a) and samples P1 (b), P2 (c), and P3 (d).

peak at 522 nm (Figure 1b). The normalized spectra reported in Figure 1b show that P1 (i.e., the ablated particles that did not receive further pulses) is considerably different from that obtained in static standard conditions, with a broader plasmonic peak at about 520 nm, slightly shifted toward longer wavelengths, and a long, broad tail in the NIR region. The spectra of P2 and P3 samples, in which the ablated nanoparticles received on average, after their formation, one or two more pulses, show a decrease of the extinction in the NIR and a narrowing of the resonance band at about 520 nm, a trend clearly moving toward the recovery of the static standard ablation extinction profile.

In TEM images (see Figure S1), one can observe a consistent fraction of anisotropic nanoparticles ("branched", BR; Figure 1d) in P1, P2, and P3 samples, which cannot be seen in the static standard synthesis (Figure 1c). About 30% of all analyzed particles in P1, P2, or P3 samples can be described as BR nanostructures. Since gold laser-ablated nanomaterials produced in diluted salt solution are stabilized by Coulombic interactions due to surface charges,[16] it can be deduced that the BR nanostructures are native structures, which are not formed after an aggregation and fusion process. Due to their anisotropic shape, equivalent diameters are defined in Figure 2 as that of a sphere having the same area of a BR nanoparticle observed in TEM images. The BR equivalent diameters were found within almost the same dimensional range of the spherical NP for all samples. This suggests that the amount of material present in BR and spherical nanoparticles is almost the same; therefore, the process generates nanoparticles with almost the same amount of material, although with different shapes. However, dynamic light scattering (DLS) measurements, reported in Figure 3, being sensitive to the hydrodynamic diameter and so to the steric hindrance, show that P1, P2, and P3 samples have distribution centered at much larger dimensions than the relative equivalent diameters obtained by TEM images, and also larger than the diameters of the nanoparticles obtained in standard conditions. The comparison of the TEM and DLS data clearly show that increasing the number of pulses, using the fluences for the ablation, the hydrodynamic size strongly reduces, with a trend toward standard gold nanoparticles usually obtained with a large number of pulses (Figure 3).

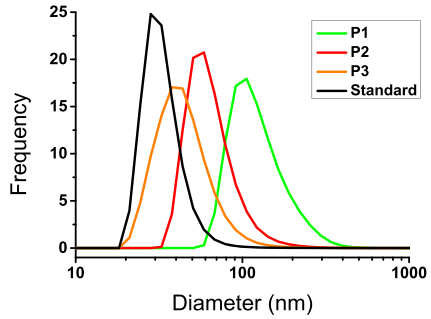

Figure 3. DLS measurement (number) of samples P1 (peak at 128 nm, 53 nm full width at half-maximum (FWHM)), P2 (67 nm, 27 nm FWHM), and P3 (46 nm, 20 nm FWHM) compared to a solution of standard gold nanoparticles (33 nm, 11 nm FWHM).

A set of simulated nanospheres and branched nanostructures were designed to elucidate the relative trend of equivalent diameters, obtained by TEM, and hydrodynamic diameters, obtained by DLS. The virtual nanostructures take inspiration from the TEM images (see Figure 4a as an example), and the complete set is reported in Figure S2. The maximum Feret diameter, namely, the nanostructure's maximum hindrance, was assumed as a fair approximation of the DLS hydrodynamic diameter. The equivalent diameters reported in Figure S2 is coherent with the definition used for TEM images, namely, the diameter of a sphere having the same volume of the relative structure. In Figure S3, the equivalent diameters and the Feret

https://dx.doi.org/10.1021/acs.jpcc.9b10793
J. Phys. Chem. C 2020, 124, 4820−4826

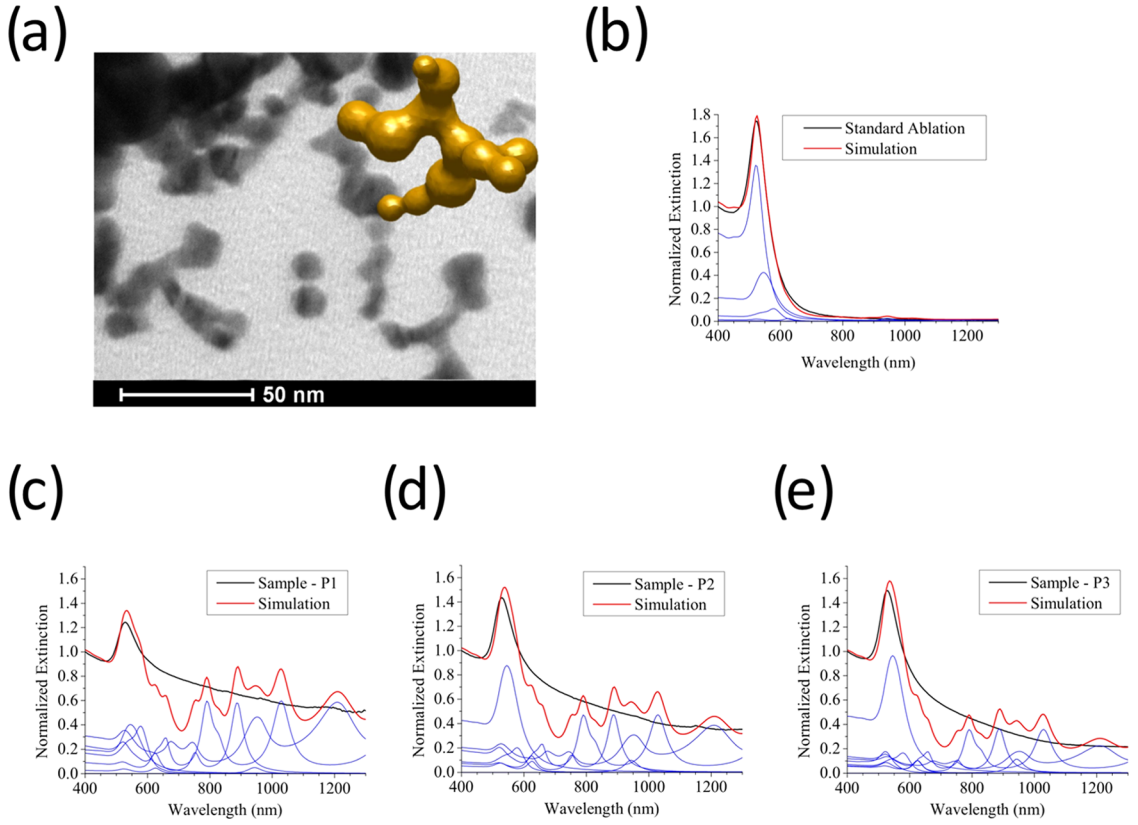

Figure 4. Simulated nanostructures were inspired by TEM images (a) and used to calculate the relative extinction spectra of single spherical nanoparticles and BR particles. The simulated extinction spectra are used as a base set to interpret the extinction spectra of AuNPs in standard static ablation condition (b), P1 (c), P2 (d), and P3 (e) as a linear combination of several contributions.

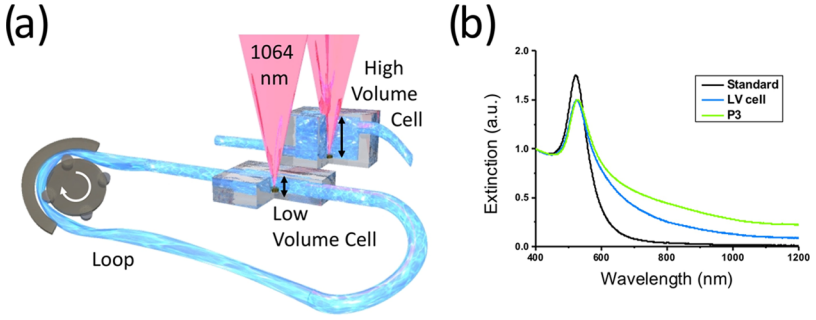

Figure 5. (a) Setup for the multipulse closed-circuit ablation. (b) Comparison between the extinction spectrum of standard gold nanoparticles, P3 sample, and the solution obtained with the close-circuit setup.

diameters are plotted together and one can see, as expected, that the two align only in case of nanospheres, while the Feret diameters diverge consistently for anisotropic nanostructures. The extinction, scattering, and absorption spectra of the same simulated geometries were then calculated using the boundary element method (BEM), thanks to the libraries published by Hohenester et al.,[28,29] and are reported in Figure S4. While the red shift of the ≈520 nm localized plasmon band is small through the series of nanospheres, the presence of new plasmon resonances in the NIR region becomes predominant as far as the nanostructure increases in both dimension (i.e., Feret diameter) and anisotropy. It should be noted that only the most branched nanostructures have consistent extinctions around 1064 nm, i.e., the wavelength used for the ablation. These results also allow interpreting the trend observed in optical measurements of samples P1, P2, and P3 in Figure 1b, since the extinction in the NIR region progressively decreases through the series. The extinction profiles obtained by BEM simulations were used for deconvolving the experimental spectra in Figure 1b, following the same approach just reported for gold nanospheres aggregates.[4] Figure 4b–e shows the normalized experimental spectra for the "standard ablation" sample and for P1, P2, and P3, together with the relative weighted simulated spectra. One first observes that the extinction contribution in the NIR region can derive almost exclusively from the BR nanostructures since none of the spherical NP shows extinctions above 800 nm. Although the simulations are obtained with a limited library of structures, the vis–NIR spectral contributions of P1, P2, and P3 samples can be clearly deduced. The overall spherical nanoparticles contribution is maximum for the standard ablation sample and minimum for the P1 sample (see Figure S5), whereas the

https://dx.doi.org/10.1021/acs.jpcc.9b10793
J. Phys. Chem. C 2020, 124, 4820–4826

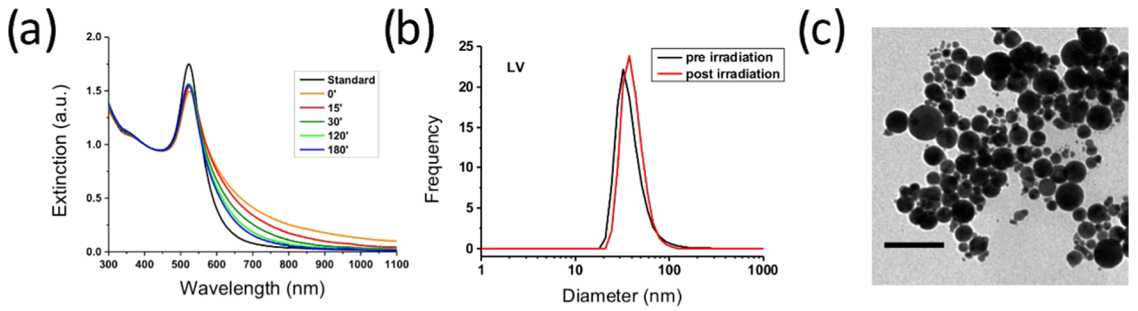

Figure 6. (a) Extinction spectra of LV cell sample during post-irradiation at times 0, 15, 30, 120, and 180 min compared with a static standard solution of ablated gold nanoparticles. (b) DLS measurement of LV sample before (peak at 39 nm, 19 nm of FWHM) and after irradiation (peak at 42 nm, 12 nm of FHWM). (c) TEM images of the closed-circuit ablation after 180 min of postsynthesis irradiation at 1064 nm. Scale bar refers to 100 nm.

opposite is found for the simulated BR contributions. In accordance with what was just achieved by observing the electron microscopy images, the trend observed with the TEM equivalent diameters and the DLS hydrodynamic diameters suggests that the pulse dosage has the effect to modulate the morphology of the ablated material toward more isotropic nanoparticles.

The conclusion that the number of pulses hitting the nanoparticles modifies, in particular, the roundness of the BR nanoparticles suggested performing in-flow ablation experiments, in which the solution circuit is closed in a loop (Figure 5a). This configuration was called "low-volume" (LV) cell because the solution over the target was only 0.5 cm high. Under this condition, the ablated material experienced multiple laser pulses. The extinction spectrum of a colloidal solution ablated for 20 min is compared, in Figure 5b, to that of P3 and of the standard nanoparticles. One finds that increasing the number of pulses is not sufficient to reproduce the extinction spectrum of the standard colloidal solution. The reason can be found in the different setup used for a standard experiment and for the looped LV cell. In particular, in a standard experiment, the liquid height over the target is 2 cm, whereas it is 0.5 cm in the LV cell. Since reshaping is usually obtained at low-fluence regimes,[30] one deduces that reshaping is obtained in the liquid above the target, where the laser beam is not focused. It can be therefore predicted to be more efficient in the static, standard setup than in the looped LV cell.

This observation suggested that to promote the nanoparticle reshaping, lower fluences are required. For this reason, a second in-flow ablation cell, in which the height of the liquid above the target was increased from 0.5 to 2 cm, was used for the ablation. This cell was called the "high-volume" (HV) cell. The fluence on the gold target surface was maintained constant at 2 J/cm^2, while, thanks to the new geometry of the HV cell, the fluence at the upper liquid surface reached a value of 0.4 J/cm^2, whereas that obtained with the LV cell was 1.4 J/cm^2. Therefore, with the HV cell, the reshaping was expected to be more efficient along the light cone of the focused beam. The vis−NIR spectra (see Figure S6a) of the looped in-flow ablation, obtained with the HV cell, confirmed the expected results showing a further reduction of the NIR tail of the extinction spectra due to the BR nanostructures. As final evidence of the reshaping mechanism of the BR nanostructures due to multiple pulses and a lower-fluence regime, the nanoparticles of the LV experiment were irradiated in a static configuration, like that of a standard ablation setup. Figure 6a shows the variation of the extinction spectrum for the LV sample, and one observes that the NIR spectral tail decreases with time, becoming more similar to that of the static standard ablated gold nanoparticles (black line). Some differences can be understood, since in the standard synthesis a plasma plume, which can interact with the particles, is always present. Both DLS measurements (see Figure 6b) and TEM images (see Figure 6c) confirm that the static irradiation of the LV sample produces more spherical nanoparticles. The same irradiation experiment was also conducted for the looped HV nanostructures, showing that the recovery of the spectral shape of the standard nanoparticles is obtained faster (see Figure S6b), as also confirmed by DLS measurement (see Figure S6c).

CONCLUSIONS

Anisotropic gold nanostructures are obtained by pulsed laser ablation under solvent when a small number of pulses are used for the ablation. Extinction spectra, supported by TEM images and DLS measurements, were used to highlight the steps that lead, in a static standard experiment, to the synthesis of spherical nanoparticles. BEM simulations supported the interpretation of the extinction spectra of the colloidal solutions, underling the different contributions of the branched (BR) and spherical nanostructures for the different types of samples. As evidenced by the results, not only the number of pulses but also the fluence profile optimization is crucial for controlling the nanostructure morphological evolution during the pulsed laser ablation process. The present study allows understanding the strategies for obtaining anisotropic nanoparticle with extinction spectra in the NIR spectral region using the laser ablation technique, which allows the synthesis of naked nanoparticles, useful for easy functionalization.

ASSOCIATED CONTENT

Supporting Information

The Supporting Information is available free of charge at https://pubs.acs.org/doi/10.1021/acs.jpcc.9b10793.

TEM images of samples P1, P2, and P3; data set of simulated structures; equivalent diameters and the maximum Feret diameters; BEM calculated extinction, absorption, and scattering spectra; overall contribution given by the virtual spherical nanostructures and the branched nanostructures; and extinction spectra of standard ablation sample compared to LV and HV sample (PDF)

https://dx.doi.org/10.1021/acs.jpcc.9b10793
J. Phys. Chem. C 2020, 124, 4820−4826

AUTHOR INFORMATION

Corresponding Authors

Lucio Litti − *Department of Chemical Sciences, University of Padova 35131 Padova, Italy;* orcid.org/0000-0001-6247-5456; Email: lucio.litti@unipd.it

Moreno Meneghetti − *Department of Chemical Sciences, University of Padova 35131 Padova, Italy;* orcid.org/0000-0003-3355-4811; Email: moreno.meneghetti@unipd.it

Author

Valentina Piotto − *Department of Chemical Sciences, University of Padova 35131 Padova, Italy*

Complete contact information is available at: https://pubs.acs.org/10.1021/acs.jpcc.9b10793

Author Contributions

The manuscript was written through contributions of all the authors. All of the authors have given approval to the final version of the manuscript.

Funding

This project was supported by P-DiSC project #04SID2016.

Notes

The authors declare no competing financial interest.

ACKNOWLEDGMENTS

The authors would like to acknowledge F. Mancin for DLS and ζ-potential measurements.

REFERENCES

(1) Bertorelle, F.; Pinto, M.; Zappon, R.; Pilot, R.; Litti, L.; Fiameni, S.; Conti, G.; Gobbo, M.; Toffoli, G.; Colombatti, M.; et al. Safe Core-Satellite Magneto-Plasmonic Nanostructures for Efficient Targeting and Photothermal Treatment of Tumor Cells. *Nanoscale* **2018**, *10*, 976−984.

(2) Litti, L.; Ramundo, A.; Biscaglia, F.; Toffoli, G.; Gobbo, M.; Meneghetti, M. A Surface Enhanced Raman Scattering Based Colloid Nanosensor for Developing Therapeutic Drug Monitoring. *J. Colloid Interface Sci.* **2019**, *533*, 621−626.

(3) Litti, L.; Reguera, J.; de Abajo, F. J. G.; Meneghetti, M.; Liz-Marzán, L. M. Manipulating Chemistry Through Nanoparticle Morphology. *Nanoscale Horiz.* **2020**, *5*, 102−108.

(4) Litti, L.; Meneghetti, M. Predictions on SERS Enhancement Factor of Gold Nanosphere Aggregates Samples. *Phys. Chem. Chem. Phys.* **2019**, *21*, 15515−15522.

(5) Pardehkhorram, R.; Bonaccorsi, S.; Zhu, H.; Gonçales, V. R.; Wu, Y.; Liu, J.; Lee, A.; Tilley, D.; Gooding, J. J. Intrinsic and Well-Defined Second Generation Hot Spots in Gold Nanobipyramids versus Gold Nanorods. *Chem. Commun.* **2019**, *55*, 7707−7710.

(6) Wang, B.; Guan, T.; Jiang, J.; He, Q.; Chen, X.; Feng, G.; Lu, B.; et al. Gold-Nanorod-Enhanced Raman Spectroscopy Encoded Micro-Quartz Pieces for the Multiplex Detection of Biomolecules. *Anal. Bioanal. Chem.* **2019**, *411*, 5509−5518.

(7) Krajczewski, J.; Kędziora, M.; Kołątaj, K.; Kudelski, A. Improved Synthesis of Concave Cubic Gold Nanoparticles and Their Applications for Raman Analysis of Surfaces. *RSC Adv.* **2019**, *9*, 18609−18618.

(8) Serrano-Montes, A. B.; Langer, J.; Henriksen-Lacey, M.; de Aberasturi, D. J.; Solís, D. M.; Taboada, J. M.; Obelleiro, F.; Sentosun, K.; Bals, S.; Bekdemir, A.; et al. Gold Nanostar-Coated Polystyrene Beads as Multifunctional Nanoprobes for SERS Bioimaging. *J. Phys. Chem. C* **2016**, *120*, 20860−20868.

(9) Khan, H. I.; Khan, G. A.; Mehmood, S.; Khan, A. D.; Ahmed, W. Gold Nanoworms: Optical Properties and Simultaneous SERS and Fl Uorescence Enhancement. *Spectrochim. Acta, Part A* **2019**, *220*, No. 117111.

(10) Szustakiewicz, P.; González-Rubio, G.; Scarabelli, L.; Lewandowski, W. Robust Synthesis of Gold Nanotriangles and Their Self-Assembly Into Vertical Arrays. *ChemistryOpen* **2019**, *8*, 705−711.

(11) González-Rubio, G.; et al. Disconnecting Symmetry Breaking from Seeded Growth for the Reproducible Synthesis of High Quality Gold Nanorods. *ACS Nano* **2019**, *13*, 4424−4435.

(12) Moreau, L. M.; Jones, M. R.; Roth, E. W.; Wu, J.; Kewalramani, S.; Brien, M. N. O.; Chen, B.; Mirkin, C. A.; Bedzyk, M. J. The Role of Trace Ag in the Synthesis of Au Nanorods. *Nanoscale* **2019**, *11*, 11744−11754.

(13) Barbosa, S.; Agrawal, A.; Rodríguez-Lorenzo, L.; Pastoriza-Santos, I.; Alvarez-Puebla, A.; Kornowski, A.; Weller, H.; Liz-Marzan, L. M. Tuning Size and Sensing Properties in Colloidal Gold Nanostars. *Langmuir* **2010**, *26*, 14943−14950.

(14) Condorelli, M.; Scardaci, V.; Urso, L. D.; Puglisi, O.; Fazio, E.; Compagnini, G. Plasmon Sensing and Enhancement of Laser Prepared Silver Colloidal Nanoplates. *Appl. Surf. Sci.* **2019**, *475*, 633−638.

(15) Fornasaro, S.; Bonifacio, A.; Marangon, E.; Buzzo, M.; Toffoli, G.; Rindzevicius, T.; Schmidt, M. S.; Sergo, V. Label-Free Quantification of Anticancer Drug Imatinib in Human Plasma with Surface Enhanced Raman Spectroscopy. *Anal. Chem.* **2018**, *90*, 12670−12677.

(16) Amendola, V.; Polizzi, S.; Meneghetti, M. Laser Ablation Synthesis of Gold Nanoparticles in Organic Solvents. *J. Phys. Chem. B* **2006**, *110*, 7232−7237.

(17) Barry, M.; Ding, B.; Jung, Y.; Reddy, B. V. K.; Phuoc, T. X.; Chyu, M. K. Pulsed Nanosecond Laser Ablation of Gold in Deionized Water and Aqueous Chitosan Solution. *Opt. Lasers Eng.* **2014**, *55*, 59−68.

(18) Giorgetti, E.; Muniz-Miranda, M.; et al. Stable Gold Nanoparticles Obtained in Pure Acetone by Laser Ablation with Different Wavelengths. *J. Nanopart. Res.* **2012**, *14*, No. 648.

(19) Link, S.; Burda, C.; Nikoobakht, B.; El-Sayed, M. A. Laser-Induced Shape Changes of Colloidal Gold Nanorods Using Femtosecond and Nanosecond Laser Pulses. *J. Phys. Chem. B* **2000**, *104*, 6152−6163.

(20) Barcikowski, S.; et al. Generation of Nanoparticle Colloids by Picosecond and Femtosecond Laser Ablations in Liquid Flow. *Appl. Phys. Lett.* **2007**, *91*, No. 083113.

(21) Menéndez-Manjón, A.; Barcikowski, S. Hydrodynamic Size Distribution of Gold Nanoparticles Controlled by Repetition Rate during Pulsed Laser Ablation in Water. *Appl. Surf. Sci.* **2011**, *257*, 4285−4290.

(22) Dittrich, S.; Streubel, R.; McDonnell, C.; Huber, H. P.; Barcikowski, S.; Gökce, B. Comparison of the Productivity and Ablation Efficiency of Different Laser Classes for Laser Ablation of Gold in Water and Air. *Appl. Phys. A* **2019**, *125*, No. 432.

(23) Letzel, A.; Santoro, M.; Frohleiks, J.; Ziefuß, A. R.; Reich, S.; et al. Applied Surface Science the Re-Irradiation of a Single Ablation Spot Affects Cavitation Bubble Dynamics and Nanoparticles Properties in Laser Ablation in Liquids. *Appl. Surf. Sci.* **2019**, *473*, 828−837.

(24) Liu, D.; Li, C.; Zhou, F.; Zhang, T.; Zhang, H.; Li, X.; Duan, G.; Cai, W.; Li, Y. Rapid Synthesis of Monodisperse Au Nanospheres Through a Laser Irradiation-Induced Shape Conversion, Self-Assembly and Their Electromagnetic Coupling SERS Enhancement. *Sci. Rep.* **2015**, *5*, No. 7686.

(25) Mafuné, F.; Kohno, J.; Takeda, Y.; Kondow, T. Formation of Gold Nanonetworks and Small Gold Nanoparticles by Irradiation of Intense Pulsed Laser onto Gold Nanoparticles. *J. Phys. Chem. B* **2003**, *107*, 12589−12596.

(26) Díaz-Núñez, P.; et al. Using Femtosecond Laser Irradiation To Grow the Belly of Gold Nanorods. *J. Phys. Chem. C* **2018**, *122*, 19816−19822.

(27) González-Rubio, G.; Díaz-Núñez, P.; Rivera, A.; Prada, A.; Tardajos, G.; González-Izquierdo, J.; Bañares, L.; Llombart, P.; Macdowell, L. G.; Palafox, M. A.; et al. Femtosecond Laser Reshaping

Yields Gold Nanorods with Ultranarrow Surface Plasmon Resonances. *Science* **2017**, *358*, 640−644.
(28) Hohenester, U.; Trügler, A. MNPBEM − A Matlab Toolbox for the Simulation of Plasmonic Nanoparticles. *Comput. Phys. Commun.* **2012**, *183*, 370−381.
(29) Hohenester, U. Making Simulations with the MNPBEM Toolbox Big: Hierarchical Matrices and Iterative Solvers. *Comput. Phys. Commun.* **2018**, *222*, 209−228.
(30) Mansour, Y.; Battie, Y.; Naciri, A. E.; Chaoui, N. Mechanisms and Advanced Photothermal Modelling of Laser-Induced Shape Transformations of Colloidal Gold Nanorods by Nanosecond Laser Pulses. *Nanoscale* **2019**, *11*, 11679−11686.

https://dx.doi.org/10.1021/acs.jpcc.9b10793
J. Phys. Chem. C 2020, 124, 4820−4826